ORIGINAL ARTICLE

Assessment of the reduction of fiber-matrix debonding in fiber-reinforced composite edge tool machining using water jets

Igor A. Shchurov [1] (ORCID) · Alexander V. Nikonov [1]

Abstract

Machining workpieces made of fiber-reinforced composites (FRC) with edge tools have a large range of applications. However, one of the drawbacks is the resulting fiber-matrix debonding in a thin layer under the machined surface. This can decrease the operational properties of the machined composite parts. A number of techniques are available to minimize machining defects in FRCs, with varying degrees of effectiveness. Fiber-matrix debonding results from the fibers having higher strength than the matrix. Consequently, during machining, the fibers bend to a greater angle compared to the matrix areas. To minimize this bending and debonding, we propose fiber counter-deflection in front of the cutting zone through water-jet pressure on the work surface. We verified this proposal using two methods: a smoothed particle hydrodynamics (SPH) simulation of the cutting process and full-scale experiments with a robotized water-jet cutting device and a special edge cutting tool. Both the calculations and the experiments generally confirmed the hypothesis of minimizing fiber debonding. Planing a FRC workpiece using water-jet pressure on the work surface provided a decrease in the length of fiber debonding by only 13% on average. This decrease is not high, but the simulations and experiments are only the initial investigations into improving the surface quality using this approach. At present, quality improvement of FRC workpiece machining with edge tools can be achieved with water-jet pressure using additional water-jet nozzles in these tools. Therefore, this paper presents the results of theoretical and experimental studies of a new technique based on the use of water jet to reduce fiber-matrix debonding.

Keywords Machining · Fiber-reinforced composites · Edge tool · Fiber-matrix debonding · Water jet

1 Introduction

A substantial number of composites, used in a range of applications [1], are fiber-reinforced composite materials (FRC), with many unidirectional composites (UD-FRC) among them [2]. In order to obtain the necessary holes, slots and grooves, parts made of UD-FRC have to be machined with edge tools [3]. During machining, the movement of the cutting tool results in a shear of the matrix and the composite fibers in the same direction. Due to the lower strength of the matrix, it is deformed more quickly, and the matrix area under the tool flank surface restores its initial position earlier. Fibers have a much higher strength and prior to cutting, their shear and bending are much greater than that of the matrix, which leads to fiber-matrix debonding [4].

Debonding is considered a defect and can be generally minimized through different methods, which can be classified in four large groups. The first group is the optimization of the cutting wedge geometry and material [5–11]. Waqar et al., using the Taguchi method, experimentally established that the rake reducing from 9° to 5° reduces the roughness from $Ra = 0.70$ μm to $Ra = 0.46$ μm [5]. They obtained results on the surface roughness increase from $Ra = 0.58$ to $Ra = 0.61$ under the variation of other tool parameters. These results are preliminary and they do not conclusively demonstrate a significant change of surface roughness under tool parameters variation. Hintze et al. established the qualitative influence of tool geometry on cutting forces and on composite damage [6]. However, their conclusions do not present numerical characteristics and the need of further research is noted. Sheikh-Ahmad indicated a significant effect of the fiber angle inclination to the work surface on fiber-matrix debonding [7]. He

✉ Igor A. Shchurov
shchurovia@susu.ru; http://www.susu.ru

[1] Faculty of Mechanical Engineering, South Ural State University, Chelyabinsk 454080, Russia

noted, "Even though the effect of rake on chip formation is minor, its effect on surface topography and machining quality in general is clear." A similar effect of other tool parameters is noted. Inoue et al. showed a 20% impact of the tool helix angle (0–45°) on surface roughness [8]. The paper stated: "this result clearly shows that the difference in the tool geometry has no effect on the finish surface." Further, the authors discuss fiber debonding, but they do not provide any solution to minimize this debonding. An attempt to modify the tool geometry to minimize fiber debonding is presented in [9]. Experimental data are not presented, however the described approach was later adopted in practice. An attempt to modify the tool geometry to minimize fiber debonding is presented in [9]. The authors used numerical calculations to obtain different patterns of fiber debonding for variable geometric characteristics of the tool. Numerical assessment of the reduction of fiber-matrix debonding is not described. In addition, experimental data are not presented. It may be concluded therefore that the authors did not find a cardinal solution to the problem. Shchurov showed the capability of Computer Numerical Control machines to tilt the tool to favorable angles to minimize fiber debonding [10]. The use of 5-axis CNC machining allowed the author to tilt the tool at favorable angle at each point of the workpiece surface. This approach has significant limitations. No numerical data noting machining process improvement are presented. The author also showed that variation of tool or working angles of the cutting tool is not a cardinal solution to the problem. Wern et al. confirmed the conclusions about the small impact of tool geometry on the machined surface quality [11]. Figure 13 of this paper shows pull-out depth change in response to rake angle variation from −20° to +20° and at the same time in response to fiber inclination angle variation from 90° to 165°. The maximal debonding, as noted by the authors themselves, was observed for the angle of fiber inclination equal to 135°. In this case, variation of fiber debonding was between 0.6 and 0.8mm. Despite the detailed description of the experimental assembly, the method for determining depth of fiber-matrix debonding is not presented. In this regard, a 25% decrease in depth of fiber-matrix debonding seems to be encouraging, but it is also not a final solution to the problem. Thus, cutting wedge geometry does not have a significant effect on the composite workpiece surface quality and further research is required.

The second group is the selection of the directions and ways of changing the primary motion and feed motion [12–14]. Lui et al., using the Taguchi method, established that the change of surface roughness from $Ra = 2.27\mu m$ to $Ra = 4.83\mu m$ is associated with increased cutting parameters [12]. However, surface roughness reflects the depth of fiber-matrix debonding only indirectly. The paper does not provide direct evidence of the relation between fiber debonding and cutting parameters. This issue requires additional study. Similar relations are noted by Nicholls et al. [13]. Xu showed that the

application of tool vibrations reduces the surface roughness from $Ra = 5.18\mu m$ to $Ra = 4.25\mu m$, a decrease of only 20% [14]. This publication presents encouraging results of application of tool vibrations. It is caused by the fact that "stresses are concentrated in a very narrow region around the tip-fiber interaction zone." At the same time, numerical data on the reduction of fiber debonding depending on the tool vibration parameters are not indicated. Thus, the problem has not yet been solved in this study. The impact of cutting parameters on the machined surface quality is obvious. An increase in the cutting parameters heightens the effect on the workpiece and reduces its quality. However, this effect is similar to that known in homogeneous material machining and is not a solution to improve machining quality.

The third group is varying the temperature of composite materials in the cutting zone [15–19]. Morkavuk et al. show that composite delamination is reduced by 2% using cryogenic exposure with different cutting data [15]. Figure 10 of the paper shows that during traditional machining delamination factor is decreased from 1.05 to 1.04 with a decrease in the feed speed from 1000 to 500mm/min, at 3000rpm spindle speed, and delamination factor is decreased from 1.045 to 1.02 with a decrease in the feed speed 1000 up to 500mm/min, at 8000rpm spindle speed. During cryogenic machining, the same indicators are decreased, respectively, from 1.036 to 1.026 and from 1.034 to 1.024. Thus, the use of cryogenics does not provide a definitive solution to the problem. Wang et al. note, "To improve the fiber cutting defects, the decrease of cutting force, the change of chip breaking method, and the drop of cutting area temperature have played a positive role in cryogenic cutting" [16]. However, the authors provided information on surface roughness and cutting forces only. In particular, the paper presents the following data on the roughness decrease depending on the temperature decrease from 293K to 103K (in μm): roughness decrease from 2.1 to 0.6 at 7000rpm, from 2.0 to 1.5 at 5000rpm, from 4.0 to 2.6 at 3000rpm, from 5.6 to 4.3 at 1000rpm. Approximately the same results are presented for feed speed variation. The authors stated surface roughness improvement up to 40%. These results show the encouraging effect of the use of cryogenics. However, no information on fiber debonding is presented in this study. This proves the need for further research on the problem. Xia et al. show that the delamination factor is increased by 11% on average [17]. Unlike the previous study, this one provides information on fiber debonding. Paradoxically, increased delamination using cryogenics is indicated. The authors note, "however, considering delamination, it does not show preferred performance within the selected drilling parameters. Further investigation is recommended…" Park et al. used the opposite effect: a laser beam was directed in front of the cutting tool [18]. The authors note, "A qualified improvement was found in the comparison of surface roughness values. There was a small decrease of

approximately 15% in the mean." Armitage et al. established that the use of a laser together with an edge tool could either reduce or increase surface roughness [19]. For the reason of this dual effect of heating the authors made a self-critical conclusion: "however further research needs to be conducted before it can be implemented in industry." Thus, workpiece cooling or heating in front of the tool provides a slight improvement in the quality and this effect also requires further study.

The fourth group is mechanical impact on the work surface in the cutting zone [20–22]. An evaluation of the impact of the counter-action on the fibers in the cutting zone using calculations was presented in [20]. The impact of a deforming wedge in front of the cutting tool was negative due to the friction force. The application of a rotating roller with projections on the periphery showed encouraging results. However, in practice, it is not possible to manufacture and use such a small roller. A similar application of the roller for wood processing reduced the surface roughness from one-and-a-half to two times [21]. Similar studies of the pre-fracture of the composite using a deforming roller showed the possibility to reduce the machined surface roughness [22]. We failed to find other studies related to mechanical impact on the work surface in front of the cutting zone. It therefore follows that this problem has hardly been studied, and its study can produce both encouraging results and the opposite data. Such research should be developed because fiber-matrix debonding in edge tool machining is a severe limiting factor to use this type of machining.

One way of treating the work surface in front of the cutting zone is to use water-jet pressure. This is logical because machining using a high-pressure water jet on the edge tool face is widely applied in metal workpieces cutting [23, 24]. The fourth group of methods is one of the most suitable for reducing fiber-matrix debonding. However, as stated above, there are practically no publications in this area. At least a preliminary assessment of this approach is required. This issue is considered in the present paper. Our research and conclusions on this issue are subject to debate. In particular, we previously studied the possibility of reducing fiber-matrix debonding in UD-FRC machining with edge tools using the deformation of the work surface in the front of the cutting zone [20]. We considered two options: using a deforming wedge (Fig. 1b, e) and using a deforming roller (Fig. 1c, f). Our studies were conducted using numeric calculation methods such as finite element analysis (FEA) and smoothed particle hydrodynamics (SPH). The adequacy of these methods for the ordinary cutting of FRC workpieces was approved in our full-scale experiments [25]. The calculations of cutting with deformation in front of the cutting zone demonstrated that friction under the deforming wedge applied on the work surface considerably pulls this zone along the cutting speed vector. This

leads to additional fiber-matrix debonding in the cutting zone.

We obtained the best results in our second simulation, with the use of a deforming roller. Rollers reduce the inclination of fibers along the cutting speed, making them more appropriate than wedges. The calculations demonstrated that fiber inclination and debonding are efficiently reduced with the use of rollers. The roller size is comparable to the size of the cutting zone. The technical realization of such a small roller is challenging. Consequently, at this stage of UD-FRC cutting studies, we can substitute rollers with a means, which would not cause considerable frictional forces on the work surface. We hypothesize that this approach can be realized using water jets (Fig. 1d), as they are widely applied in machining with edge cutting tools. Many serially produced cutting tools have internal coolant system for pressurized liquid supply and modern machine tools also have the necessary equipment for liquid supply.

The effect of such water jets on fiber debonding can be studied both theoretically and experimentally. At present, theoretical studies of similar processes tend to be carried out using numerical calculation methods, including the finite element method and mesh-free methods, such as SPH. In a recent study Gök rightly points out, "the success and reliability of numerical models are heavily dependent upon the work-material-flow stress, friction parameters for the tool and work-material interfaces, the fracture criterion and thermal parameters" [26]. This study achieved its objectives using a homogeneous material – steel. However, for UD-FRC machining simulation calculations are much more complicated. Modeling is frequently carried out without regard to fiber-matrix boundary interface [9, 10]. However, it is this zone, where matrix characteristics are very special, and therefore it is here where fiber debonding takes place. The authors have previously carried out FEM calculations of UD-FRC machining [27] taking into account boundary interface. However, FEM problems connected with mesh fragmentation in such layers by means of removing elements due to the mass loss failed to produce adequate results. Similar studies were described by Li et al. [28]. Here, the authors also used the failure criteria of ultimate stresses and strains. The scale of stress distribution makes it impossible to define the modeling method of fiber-matrix debonding; apparently, it is similar to the previous method—removing finite elements of the interfaces. In other studies [29, 30] the boundary layer is modeled using thin solid elements and the authors use different failure criteria for assessing the stages of debonding process. However, the feature of FEM connected with removing destroyed elements in this case also leads to inaccurate results. The SPH modeling does not have this drawback. A recent study presented the results of modeling UD-FRC cutting using both calculation methods [31]. Figure 29 of this study presents a clear difference in the volumes of chips in both cases, which demonstrates that
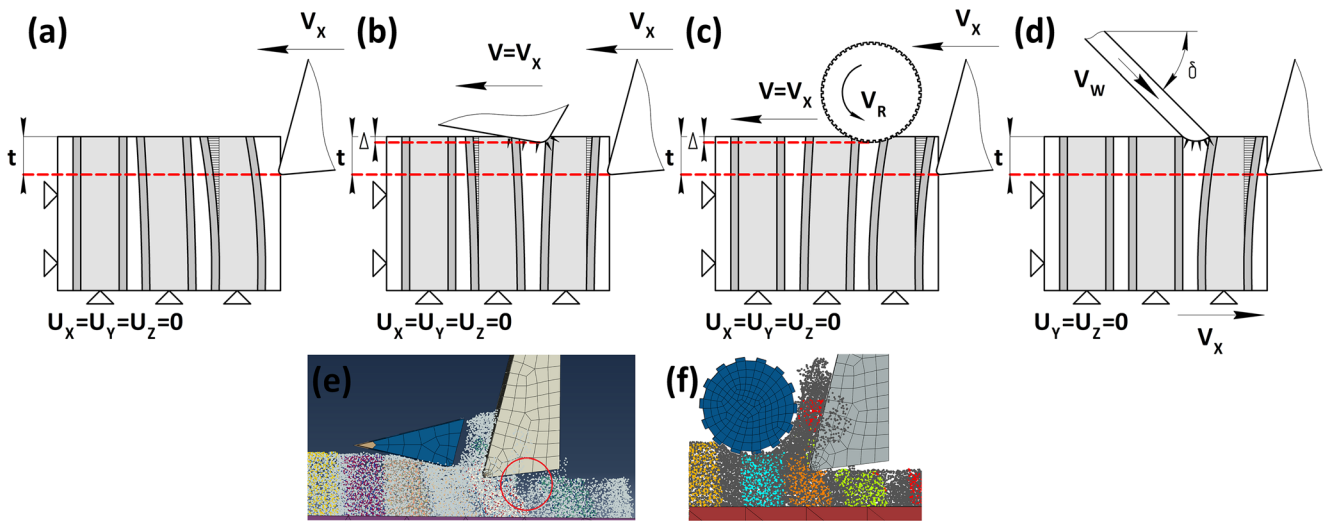
Fig. 1 Methods of the preliminary deformation of the cutting zone in front of the cutting wedge ((**a**) traditional cutting, (**b**) cutting with the use of a deforming wedge, (**c**) cutting with the use of a deforming roller, (**d**) cutting with the use of a water jet), and SPH simulations: work surface deformation in front of the cutting zone using (**e**) a deforming wedge and (**f**) a roller [20]

the SPH method is more suitable. The mutual effect of a tool wedge and a water jet was beyond the scope of that paper, however. There are studies focused upon hydroabrasive treatment [32–34]. These studies use the SPH and the FEA to simulate workpiece cutting into two parts. The alternative to SPH for modeling liquids under pressure is the Arbitrary Lagrangian Eulerian (ALE) method [35], which according to [36] is also effective but has some limitations, large displacements and deformations, resulting in the need for mesh regeneration. The problem complexity is increased by an order of magnitude consequently. As a result, similarly to edge tool machining simulation, we can observe a significant influence of the calculation method (ALE or SPH) and the parameters of the workpiece. All this demonstrates the necessity of further research. Since the issue of machining UD-FRC using the combination of an edge tool and water jet pressure has not yet been studied, the theoretical studies of SPH application taking into account the abovementioned features are highly relevant.

The purpose of this study is to increase the quality of the surface layer of the UD-RFC workpiece by minimizing fiber debonding from the matrix by treating the work surface with a water jet directly in front of the chip formation zone. This approach can be realized by solving two tasks. The first is a preliminary assessment of the feasibility of this approach through computer simulations using FEA-SPH modeling of chip formation in a composite workpiece with the application of a moving water jet. This task is described in Section 2. The second task is to conduct full-scale experiments to prove the hypothesis and provide qualitative proof of the simulations. These results are presented in Section 3. The discussion of the results and conclusions are given in the final sections.

2 FEA-SPH simulation of UD-FRC workpiece machining using a water jet moving in front of the cutting zone

2.1 Problem setting and model parameters

Numerical simulation of cutting was performed in LS-DYNA. A bar of UD-FRC consisting of carbon fiber AS4 ($1800 kg/m^3$ density [37]) with the orientation angle of 90° and epoxy matrix MTM45-1 ($1160 kg/m^3$ density [37]) was used as a workpiece. The LS-DYNA card MAT_COMPOSITE_DAMAGE [38] for the modeling of orthotropic material, which is subject to brittle failure, was applied in the simulation. Orthotropic linear elasticity and Chang-Chang failure criteria were used for this study [39, 40].

In order to account for the contact fiber-matrix interaction, we placed a boundary layer, the parameters of which are identical to those specified for the matrix, excepting shear modulus 1GPa and Young's modulus 2 GPa. The material of the tool was considered to be absolutely rigid. The rest parameters are provided in Table 1.

For the water-jet simulation we chose card Null-Material model in LS-DYNA and the Grüneisen equation of state in Eq. 1 (refer to Ref. [38]). The parameters of the water jet are provided in Table 2 [41].

$$\rho = \frac{\rho_0 C^2 \mu \cdot \left[1 + \left(1 - \frac{\gamma_0}{2}\right) \cdot \mu - \frac{\alpha}{2} \cdot \mu^2 \right]}{\left[1 - (S_1 - 1) \cdot \mu - S_2 \cdot \frac{\mu^2}{\mu + 1} - S_3 \cdot \frac{\mu^2}{(\mu + 1)^2} \right]} + (\gamma_0 + \alpha\mu) \cdot E \qquad (1)$$

where ρ_0 is the initial density, C is the speed of sound, γ_0 is the Gruneisen gamma, α is the volume correction coefficient, S_1,

Table 1 Parameters of a model

Element	Parameter	Value
Processing modes	Cutting depth, mm	1
	Cutting speed, m/min	0.3
Cutting tool	Tool rake γ, deg.	10
	Tool clearance α, deg.	5
	Rounded cutting edge radius R, mm	0.3
Workpiece	Length, mm	11.5
	Height, mm	10
	Reinforcement angle, deg.	90
	Fiber diameter, mm	1
	Distance between fibers, mm	2.5
Water jet	Angle of inclination in relation to the work surface, deg.	45
	Diameter, mm	1
	Speed, m/s	600

S_2, and S_3 are fitting coefficients, and E denotes the internal energy, which is increased according to an energy deposition rate as a function of time curve, and dimensionless parameter:

$$\mu = \frac{\rho}{\rho_0} - 1, \tag{2}$$

where ρ is the current density.

While modeling a cutting wedge, we chose Belytschko-Tsay Shell elements for the rigid body (ELFORM=2) [38], shell thickness 0.1mm, and element size 0.25mm. The workpiece and a water jet were modeled with the help of SPH elements. Cubic spline kernel function and default formulation of particle approximation theory were used in the simulation. Bucket sort based algorithm was used for computation of the smoothing length. Monaghan type artificial viscosity formulation was used for SPH elements. Relative particles distance was equal to 0.25mm.

In the simulation, the test specimen was moved at a constant speed towards a firmly fixed cutting wedge. Workpiece lower bound was rigidly fixed along Y and Z axes. This bound

Table 2 Initial parameters of the water jet [41]

Parameter	Value
Density, kg/m^3	1000
Pressure cutoff, Pa	-10^5
Coefficient of viscosity, Pa s	0,001
Bulk sound speed in a material, m/s	1480
Coefficient $S1$	2.56
Coefficient $S2$	−1.986
Coefficient $S3$	0.2286
Grüneisen coefficient	0.4934
Parameter A	1.397

was moved towards the cutting wedge (along the X-axis) at $\overrightarrow{V}_x$ speed. The water jet was flowed at a constant initial speed in front of the cutting zone near the edge. The vector of the water jet was directed at an angle of 45° to the work surface. The workpiece moving was used due to the limited capacity of the experimental assembly, particularly the difficulties connected with ensuring the synchronization of the movements of the cutting tool and the water-jet nozzle. This scheme will further be implemented on an edge tool equipped with internal coolant system. The modeling of the machining with the use of the water jet is shown in Fig. 2. The simulation model parameters are provided in Table 3.

2.2 Simulation results

Figures 3 and 4 present the results of the cutting simulation, notably the planing of the UD-FRC workpiece. We provide the results of simulations with and without the use of the water jet. The simulation results show the tool consistently contacting different fibers, which is accompanied with sharp increase in strains propagating along the fibers being cut and adjacent fibers (Fig. 3). The cutting wedge sequentially folds back the reinforcing fibers that debone at the fiber-matrix interface until the bending strength is exceeded. For each fiber, destruction first spreads along the fiber-matrix interface and then orthogonally to this fiber. In dry cutting, fiber fracture, which is brittle takes place slightly lower than the contact point with the cutting edge, and corresponds to expectations [47].

Chip formation is accompanied by shear deformations along the fiber axes caused by compression, when the shear destruction of the boundary layer takes place. According to the simulation results, we can differentiate the following main types of machined surface damage during carbon fiber FRC cutting. The types are also presented in Fig. 4a:

Fig. 2 FEA-SPH model

Table 3 Parameters of materials

| Material	Parameter		Value	UoM	Source
Carbon fiber (AS4)	Density		1800	kg/m^3	[37]
	Elastic constants	Young's modulus X direction. E1	231	GPa	[42]
		Young's modulus Y direction. E2	15	GPa	[37]
		Young's modulus Z direction. E3	15	GPa	[37]
		Poisson's ratio XY. v21	0.02	-	[37]
		Poisson's ratio YZ. v31	0.02	-	[37]
		Poisson's ratio XZ. v32	0.4	-	[37]
		Shear modulus G12	15	GPa	[37]
		Shear modulus G31	15	GPa	[37]
		Shear modulus G23	7	GPa	[37]
	Tensile strength	Xt	4620	MPa	[42]
		Yt	1500	MPa	[42]
	Compressive strength	Xc	3960	MPa	[37]
		Yc	3340	MPa	[43]
	Shear strength	S	1500	MPa	[44]
Epoxy (MTM45-1)	Density		1160	kg/m^3	[37]
	Elastic constants	Young's modulus E	3.35	GPa	[37]
		Poisson's ratio v	0.35	-	[37]
		Shear modulus G	1.4	GPa	[45]
		Bulk modulus	4.2	GPa	[46]
Interface	Density		1565	kg/m^3	-
	Elastic constants	Young's modulus E	2	GPa	-
		Poisson's ratio v	0.35	-	-
		Shear modulus G	1	GPa	-
		Bulk modulus	3	GPa	-
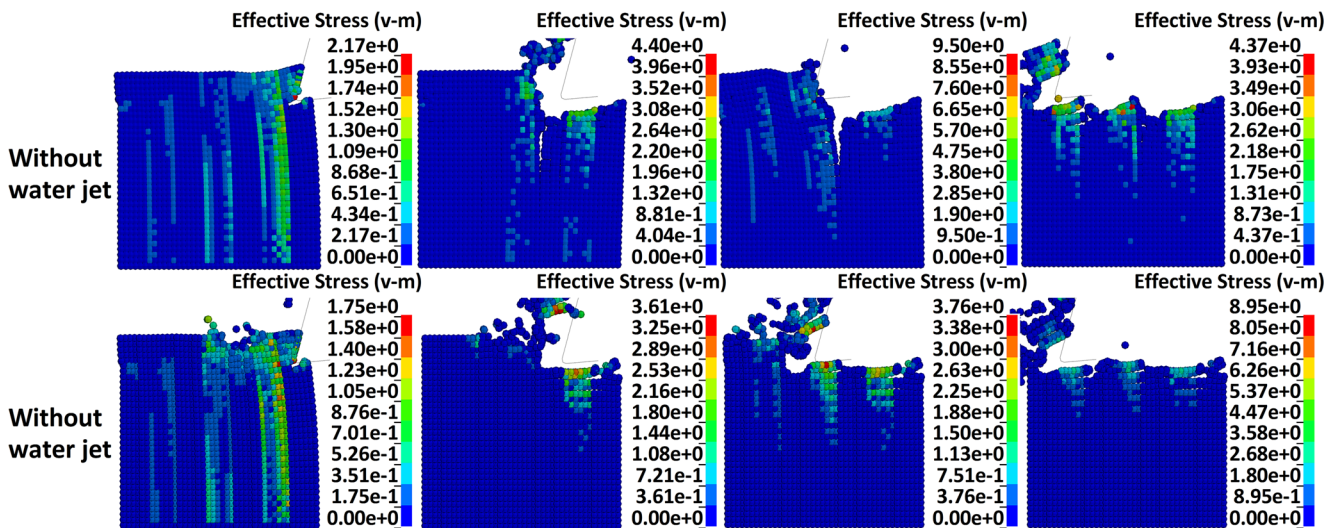
Fig. 3 Results of the numerical simulation: cutting without water jet and with water jet (von Mises stress pattern)

– Debonding caused by the pressure effect of the cutting wedge on the fiber, which leads to the crack-face contact propagation;
– Chipping, caused by the brittle destruction of the surface layer, accompanied by reinforcing fibers separation together with fragments of the destroyed matrix;
– Fiber rebound caused by strain recovery which decreases the actual depth of cut by Δt.

In the case of water-jet machining, the cutting wedge tends to bend fibers in the direction opposite to the cutting speed vector $\vec{V}_x$ (movement of the workpiece). The supporting force, created by the water jet prevents this

tendency. This water jet deforms the area in front of the cutting wedge, which can be proved by the propagation of stresses in the zone located in front of the wedge (Fig. 3). It also ensures the support of fibers during cutting, resisting their bending deformation in the opposite direction from the cutting wedge movement. Therefore, the degree of crack-face contact propagation along the fiber-matrix interface is decreased by 20…40% compared to traditional cutting (Fig. 4a). Fiber destruction, in contrast to dry cutting, takes place at the contact point with the cutting edge, which minimizes chipping.

Figure 4b demonstrates that the components of the cutting force are reduced approximately by half during water-jet
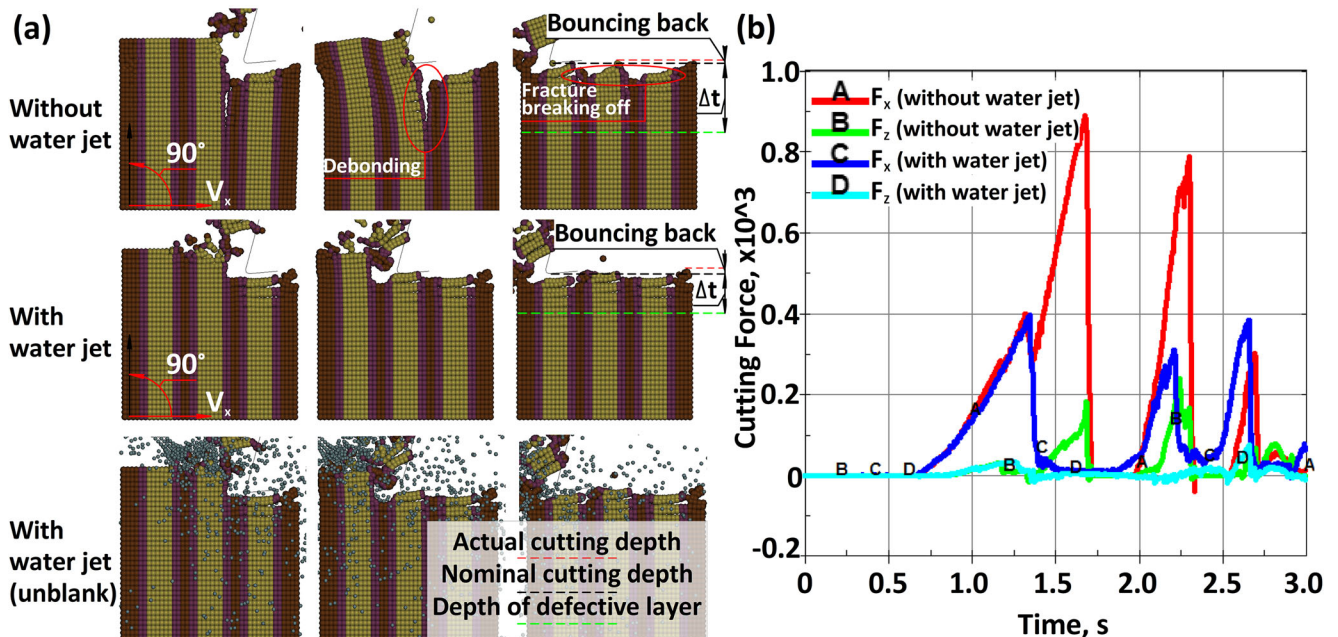

Fig. 4 Results of numerical simulation: cutting without water jet and with water jet ((**a**) cutting process simulation, (**b**) cutting forces)

cutting, which can be explained by the better conditions for cutting the fibers near the cutting edge.

Figure 5 shows the results of the equivalent stress calculation on fiber boundaries. The points, where stresses were measured, are marked by A…L. Unfortunately, unlike FEA, no cohesive model can be implemented when the SPH method is used. Therefore, information on the fiber-matrix interface cannot be obtained. Thus, the depth of debonding was assessed indirectly through the observation of stresses along the fiber-matrix interface. The graphs demonstrate that sharp increase of stresses happens at the moments prior to fiber destruction, which corresponds to expectations. Three sharp increases of stresses can be observed. During dry cutting, the first increase is caused by the beginning of cutting the previous fiber, the second increase, by the maximum impact of the previous fiber at the moment prior to its separation, the third increase, at the moment of the greatest bending and subsequent separation of the fiber. During water-jet cutting the first increase takes place when the water jet contacts with the work surface, the second increase is caused by maximum impact of the previous fiber at the moment prior to its separation and the third increase, at the moment of fiber separation. For water-jet cutting, the time interval between the second and the third increases is longer compared to dry cutting, which proves there are less fiber bending and consequently less depth of debonding. These figures prove that a high-pressure water jet considerably reduces equivalent stresses in the layer under the machined surface compared to dry cutting.

3 Experimental study of a UD-FRC workpiece machining using a water jet moving in front of the cutting zone

3.1 Equipment and experimental procedure

We conducted an experiment to investigate machining using a water jet moving in front of the cutting zone. We prepared special UD-FRC workpieces produced for the experiment (Fig. 6, inset). The matrix was produced using a binding agent consisting of Etal-370 resin and Etal 45-M hardener. High-modulus glass fiber T-60/2(BMΠ)-14 with the fiber orientation angle ±90° was chosen for study. The test specimens were produced using the hot-press method and consisted of 10 layers of glass fiber 0.16 mm each (arranged in the same direction). First, the workpiece was cut using a DIADISC 4200 circular saw produced by Mutronic. Then, to guarantee the workpiece surface quality we used fine-grit sandpaper (P2000 ISO/FEPA) attached to a flat metal surface.

The experiment on UD-FRC cutting was conducted using AWJet Robotics 3020, a robotic system for water-jet cutting. The purpose-made experimental assembly was table mounted (Fig. 6, main image).

The assembly consisted of a movable carriage with an electric motor. A device for fixing the composite workpiece was mounted on the carriage. The carriage speed was 100mm/min. The robotic system table had an additional fixture to hold a 2120-0066 GOST 18881-73 single-point cutting tool. The tool had a tungsten carbide insert with geometric parameters presented in Section 2. Figure 7 shows UD-FRC machining
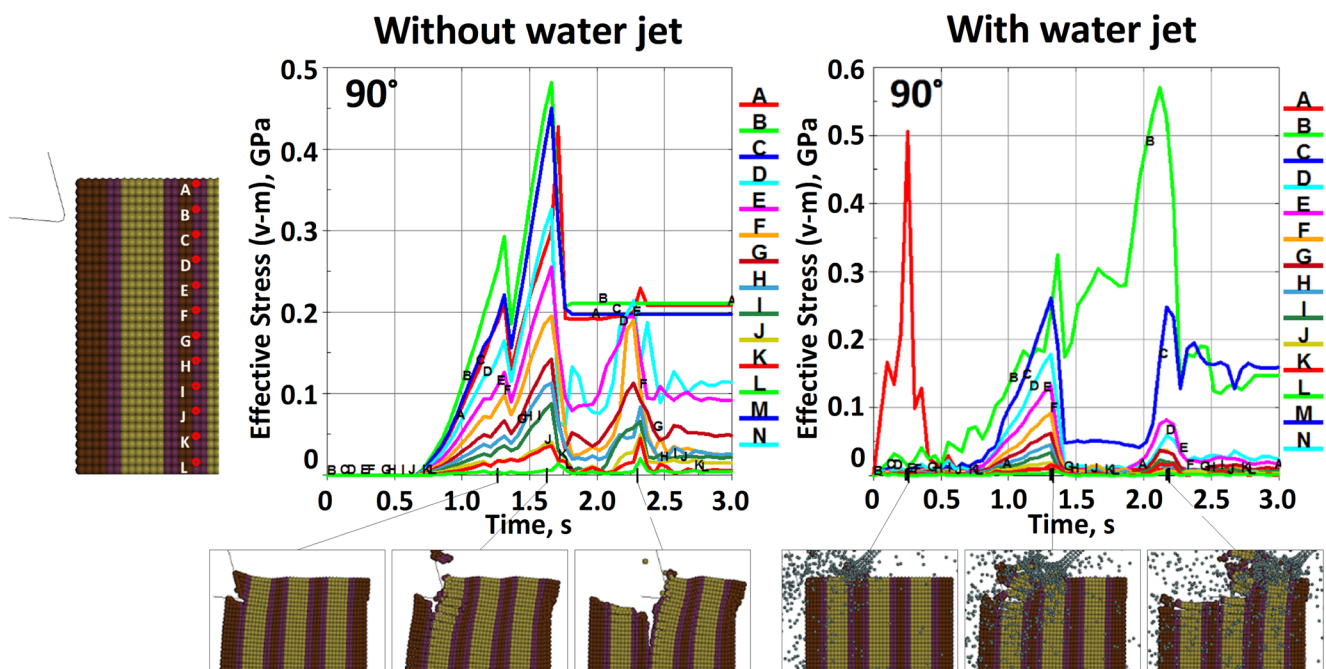

Fig. 5 Change of equivalent stress in points along fibers and at different times of cutting with and without water jet
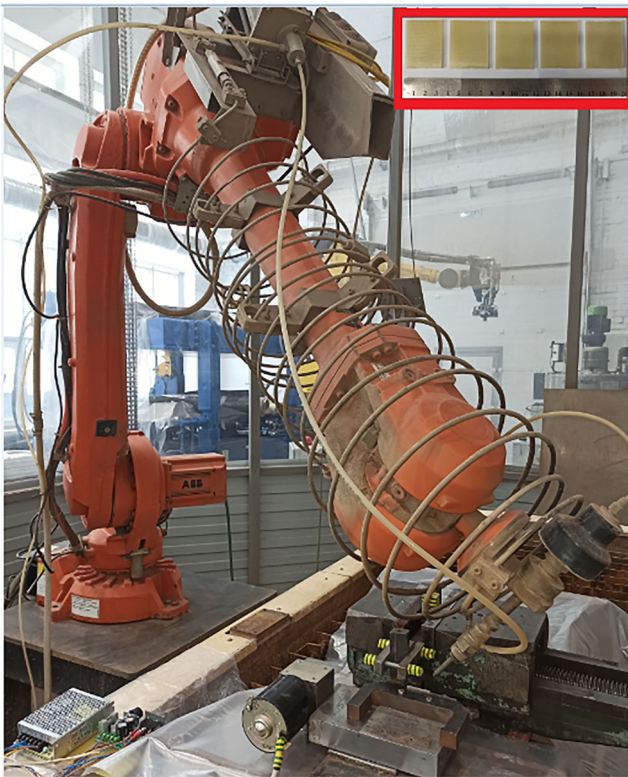
Fig. 6 Experimental assembly. AWJet Robotics 3020 with special devices, the cutting tool and the workpiece. Workpieces are presented in the inset at the top right

without water-jet (left) and with (right). The cutting head of the robotic system was used for the water flow. The cutting head had a 7.14×1.02×76 injector and a ruby nozzle with a 0.3mm diameter hole. The water flow rate was 0.01kg/s at a jet speed of 150m/s. Using this assembly, we machined several workpieces with and without water jets.

The surfaces of the machined composite workpieces were checked using the liquid penetrant inspection method. Initially, we mechanically removed the outer layers of the test

specimens, which are not indicative. The absence of layer side support caused additional fiber separation from these layers.

Therefore, the layers were removed in three stages: (1) rough polishing with a 140x70x3 diamond needle file, MATRIX MASTER 15835; (2) fine-grit sandpaper (P2000 ISO/FEPA Grit designation) treatment; (3) polishing using a felt wheel with GOI polishing paste №2 TU 6-18-36-85 (RU). Further, the surfaces were cleaned with AEROPEN-KD LR-2. After this preparation, red penetrant AEROPEN-KD RF-1 was spread on the pre-polished surfaces. After penetration and drying, the excess penetrant was removed. The depth of the defect layer was measured using a Digital Microscope 1600X and the software CoolingTech MicroScope.

3.2 Results

The test specimens before and after machining are shown in Fig. 8. Microscope images are given in Fig. 9. Image processing was done using the Fiji program [48]. The processing was as follows: the original microscope images were subjected to color correction using the Fiji program to increase the contrast and then converted into raster images. Then, using the Fiji software tools, the areas of the defect zones (delamination, chipping, fracture, breaking off, porosity, mashing, cracking) were measured.

During the experiment, we observed that in dry cutting, fibers, which have a much higher strength than the matrix at the contact with the cutting wedge, are bent very significantly because of the lack of additional support. The result of this is cracks propagation along the fiber-matrix interface. Later, the cutting process demonstrates fiber pull-out, which increases the depth of the defect layer and reduces the quality of the machined surface. The introduction of the water jet reduced fiber bending due to the support during machining, decreased the size of the defect zone and improved the quality of the

Fig. 7 Experimental assembly: without water jet (left) and with water jet (right)

Fig. 8 Test specimens before (**a**) and after the machining (without (**b**) and with (**c**) water jet)
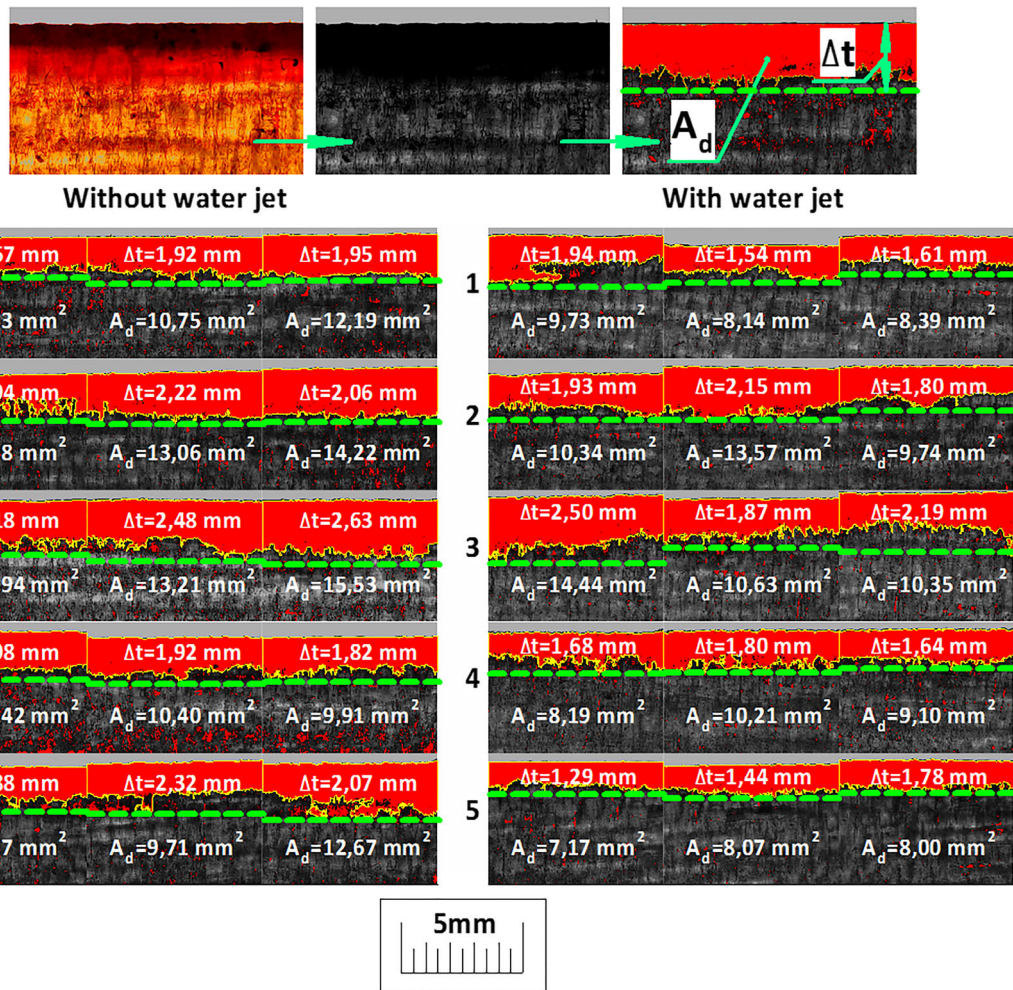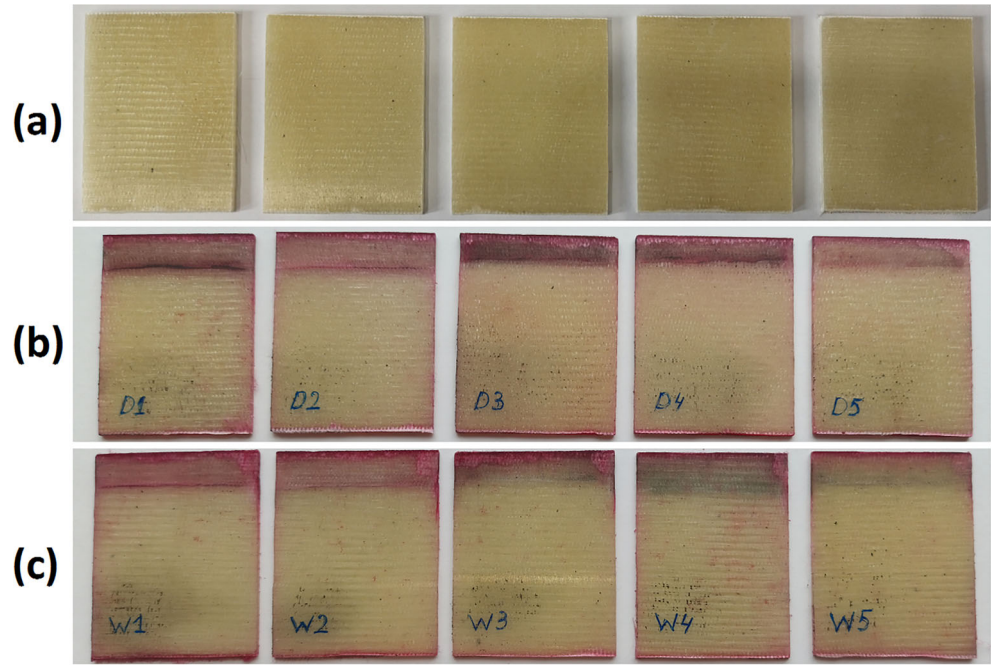

Fig. 9 Image processing stages to determine the areas of the defect zones *Ad* and depth of the defect layer *Δt* (top), and defect UD-FRC zones areas (1–5): dry cutting (left)—A_{d1}; cutting with water jet (right)—A_{d2}

surface layer. Figure 9 shows that cutting with a water jet reduced the defect zones areas by $\mathrm{Mean}(100(A_{d1} - A_{d2})/A_{d1}) = 16\,\%$.

The depth of the defect layer Δt decreased by 13% with water-jet cutting. This significant discrepancy between the theoretical and experimental data is presumably caused by insufficient accuracy of the experimental procedure: the penetrant dye does not fill thin debonding zones in the lower part of the surface layer of the workpiece and does not allow us to accurately define fiber debonding in this area. Thus, the underestimated values of experimental data seem less promising but more reliable.

This points to the effectiveness of the proposed method and proves the hypothesis of our study.

4 Discussion and future work

The experiments were not intended to be exhaustive. Later, in the study of other composite materials (fiber-reinforced polymers, metal matrix composites or ceramic matrix composites) other results may be obtained. Probably, in some of these studies, the effect will either not appear, or may be the opposite. We have not examined the correlation between the degree of fiber debonding and the angle of fiber inclination to the work surface. We have not studied various configurations of the reinforcing structure yet. Our calculations were performed using specific parameters of the numerical model; simulation success is heavily dependent upon them [26]. It is important that variation of material models parameters was not examined. Parameter values presented by other researchers of materials were used [37, 41, 42, 44, 45, etc.]. We performed a numerical simulation of cutting certain UD-FRC with certain cutting tools. We considered certain cutting modes and water jet parameters. The final results of the simulation would have been affected by the use other composites, tools, and cutting mode parameters. However, these original calculations are the positive result. They prove the possibility to use a water jet to reduce fiber-matrix debonding under certain conditions. The achieved improvement is not a definitive solution to the problem. However, the degree of this improvement is comparable to the results from other studies. The degree of crack-face contact propagation along the fiber-matrix interface is decreased by 20...40% compared to traditional cutting. For example, improvement of workpiece surface quality by changing the tool geometry ranged from 20% [8] to 40% [5]. Workpiece surface quality improvement by the change of the cutting parameters varied from 20% [15] to 50% [12]. However, the surface quality was characterized by surface roughness, which is only indirectly related to fiber debonding. Contradictory information on

the effect of thermal [5–19] and mechanical [20–22] impacts and the depth of fiber-matrix debonding comparable to our results lead us to the general conclusion: our theoretical studies of water jet application are encouraging and require further research.

The same may be said of the experiment: the range of parameters was limited. It was difficult to set the necessary jet diameter, supply area, and supply angle. We are concerned that the decrease in the depth of the defect layer was not as significant as the decrease in the SPH simulation. We think that this is related to the drawback of the method of experimental determination of the debonding length. The penetrant could not leak in thin gaps and demonstrate the real depth of debonding. Unfortunately, there is no information on experimental methods for determining this parameter in the published studies. Therefore, our experimental method is a matter of discussion. However, our hypothesis was experimentally proved in general. The surface layer of the machined composite workpiece was improved.

Additional experiments are necessary to establish the links between the geometry of cutting tool wedges and the parameters of the composites, cutting mode parameters, and specificities of the water jet supply. It is also necessary to design water jet nozzles for various cutting tools (single-point cutting tools, milling cutters, drills) with the best nozzle location and to set the necessary water pressure. At present, tools with internal coolant systems are widely used for the improving of chip formation in metal cutting. Numerical control machines are equipped with high-pressure pumps to supply coolant water at the tool corner. Consequently, it will not be difficult to use new tools with other, similar nozzles for cutting FRC workpieces. All of these will make it possible to minimize the destruction of composite surface layers during edge tool machining.

5 Conclusions

This paper presents only the initial stage of investigations into minimizing the destruction of composites in machining with edge tools using a high-pressure water jet. However, even at this initial stage we can draw the following conclusions:

1. The SPH-simulation and experimental studies of FRC workpiece cutting proved the significant reduction of fiber-matrix debonding during edge tool cutting using a water jet moving in front of the cutting zone (compared to other known methods, e.g. optimization of wedge geometry, processing mode and thermal impact).

2. SPH calculations proved that the destruction of the composite fiber with a cutting wedge when dry cutting takes place lower than the contact point with the cutting edge, which corresponds to expectations, whereas the

destruction of fiber with a cutting wedge during water-jet cutting takes place at the contact point with the cutting edge, which explains the reduction of fiber debonding below this point.

3. SPH calculations proved that sharp increase of stresses along the fiber-matrix boundaries take place at the moments preceding the destruction of fiber, which corresponds to expectations. Three sharp increases of stresses can be observed. When dry cutting, the first increase is caused by the start of cutting the preceding fiber, the second increase is caused by the maximum impact of the preceding fiber at the moment prior to its separation, the third increase happens at the moment of the greatest bending and further separation of the fiber under consideration. When water-jet cutting, the first increase is caused by the contact of the water jet with the work surface, the second increase is caused by the maximum impact of the preceding fiber at the moment prior to its separation and the third one at the moment of separation of the fiber under consideration. The time interval between the second and the third increases during water-jet cutting is longer compared to dry cutting, which proves there are less fiber bending and, consequently, less depth of debonding for water cutting.

4. The SPH simulation showed that using a water jet reduces fiber debonding by 20–40% compared to dry cutting. Experimental studies proved that using a water jet reduced the depth of the defect layer by 13% and the defect zone area by 16%. This significant difference between the theoretical and experimental data can presumably be explained by the insufficient accuracy of the experimental measurement: a penetrant-dye does not fill thin zones of debonding in the lower part of the surface layer of the workpiece and does not make it possible to accurately define fiber debonding depth in this area. The underestimated values of experimental data seem less promising but more reliable.

Nomenclature FEA, Finite element analysis; FEM, Finite element method; FRC, Fiber-reinforced composites; SPH, Smoothed particle hydrodynamics; UD-FRC, Unidirectional fiber-reinforced composites; ALE, Arbitrary Lagrangian Eulerian

Code availability Not applicable.

Data availability Not applicable.

Declarations

Ethics approval and consent to participate Not applicable.

Consent for publication Not applicable.

Competing interests The authors declare no competing interests.

References

1. Hu N (2012) Composites and their applications. IntechOpen. https://doi.org/10.5772/3353
2. Campbell FC (2010) Structural composite materials. ASM International, Materials Park, Ohio
3. Caggiano A (2018) Machining of fibre reinforced plastic composite materials. Materials (Basel) 11(3):442. https://doi.org/10.3390/Fma11030442
4. Teti R (2002) Machining of composite materials. CIRP Annals 51(2):611–634. https://doi.org/10.1016/S0007-8506(07)61703-X
5. Waqar S, He Y, Abbas CA, Majeed A (2017) Optimization of cutting tool geometric parameters in milling of CFRP laminates. 21st International Conference on Composite Materials
6. Hintze W, Hartmann D (2013) Modeling of delamination during milling of unidirectional CFRP. Procedia CIRP 8:444–449. https://doi.org/10.1016/j.procir.2013.06.131
7. Ahmad J (2009) Machining of polymer composites. Springer US
8. Inoue T, Hagino M, Tokuno K, Usuki H, Miyamoto J (2015) The machinability of CFRP with cutting movement of end-milling. Key Eng Mater 656-657:391–397. https://doi.org/10.4028/www.scientific.net/KEM.656-657.391
9. Shchurov IA, Nikonov AV (2016) Fiber-reinforced composite workpiece surface quality improvement in machining by milling-cutter with opposite cutting edges using SPH-method simulation. Bulletin of the South Ural State University. Ser Mech Eng Ind 16(1):56–62. https://doi.org/10.14529/engin160104
10. Shchurov IA (2015) A method of improving fiber-reinforced composite workpiece surface quality during the machining on 5-axis CNC machines. Procedia Eng 129:99–104. https://doi.org/10.1016/j.proeng.2015.12.015
11. Wern CW, Ramulu M, Shukla A (1996) Investigation of stresses in the orthogonal cutting of fiber-reinforced plastics. Exp Mech 36:33–41. https://doi.org/10.1007/BF02328695
12. Liu G, Chen H, Huang Z, Gao F, Chen T (2017) Surface quality of staggered PCD end mill in milling of carbon fiber reinforced plastics. Appl Sci 7(2):199. https://doi.org/10.3390/app7020199
13. Nicholls CJ, Boswell B, Davies IJ, Islam MN (2017) Review of machining metal matrix composites. Int J Adv Manufact Technol 90:2429–2441. https://doi.org/10.1007/s00170-016-9558-4
14. Xu W, Zhang LC, Wu Y (2014) Elliptic vibration-assisted cutting of fiber-reinforced polymer composites: understanding the material removal mechanisms. Compos Sci Technol 92:103–111. https://doi.org/10.1016/j.compscitech.2013.12.011
15. Morkavuk S, Köklü U, Bağcı M, Gemi L (2018) Cryogenic machining of carbon fiber reinforced plastic (CFRP) composites and the effects of cryogenic treatment on tensile properties: a comparative study. Compos Part B: Eng 147:1–11. https://doi.org/10.1016/j.compositesb.2018.04.024
16. Wang F, Wang Y, Hou B, Zhang J, Li Y (2016) Effect of cryogenic conditions on the milling performance of aramid fiber. Int J Adv Manufact Technol 83:429–439. https://doi.org/10.1007/s00170-015-7574-4
17. Xia T, Kaynak Y, Arvin C, Jawahir IS (2016) Cryogenic cooling-induced process performance and surface integrity in drilling CFRP composite material. Int J Adv Manufact Technol 82:605–616. https://doi.org/10.1007/s00170-015-7284-y
18. Park CI, Wei Y, Hassani M, Jin X, Lee J, Park SS (2019) Low power direct laser-assisted machining of carbon fiber-reinforced polymer. Manufact Lett 22:19–24. https://doi.org/10.1016/j.mfglet.2019.10.001
19. Armitage K, Masood S, Brandt M, Pomat C (2004) Laser assisted machining of hard-to-wear materials. Technical Report to Weir Warman Ltd, Industrial Research Institute Swinburne 155-161.

20. Shchurov IA, Nikonov AV, Boldyrev IS (2016) SPH-Simulation of the fiber-reinforced composite workpiece cutting for the surface quality improvement. Procedia Eng 150:860–865. https://doi.org/10.1016/j.proeng.2016.07.029

21. Grabar IG, Fryshev SG, Kulman S (2017) Some features of rheological behavior of wood at milling. Sci Bull UNFU 27(1):142–144. https://doi.org/10.15421/40270132

22. Yaroslavtsev VM (2018) Intensification techniques for polymer composite material processing. Vestn Mosk Gos Tekh Univ im N E Baumana, Mashinostr 6:60–71. https://doi.org/10.18698/0236-3941-2018-6-60-71

23. Kerrigan K, Scaife RJ (2018) Wet vs dry CFRP drilling: influence of cutting fluid on tool performance. Procedia CIRP 77:315–319. https://doi.org/10.1016/j.procir.2018.09.024

24. Anan R, Matsuoka H, Ono H et al (2017) A study examining the effects of water-miscible cutting fluids for end milling process of carbon fiber reinforced plastic. AIP Conference Proc 1835:020032. https://doi.org/10.1063/1.4981854

25. Shchurov IA, Nikonov AV (2019) SPH modeling and experimental study of unidirectional fiber-reinforced composite cutting. Proceedings of the 4th International Conference on Industrial Engineering. ICIE 2018. Lect Notes Mech Eng 1631-1638. https://doi.org/10.1007/978-3-319-95630-5_174

26. Gök A (2017) 2D numeric simulation of serrated-chip formation in orthogonal cutting of AISI316H stainless steel. Materials And. Technology 51(6):953–956. https://doi.org/10.17222/mit.2017.038

27. Shchurov IA, Boldyrev IS (2012) Finite element method calculation of free orthogonal cutting of composite materials. Bull South Ural State Univ, Series "Mech Eng Ind" 12:143–147

28. Li NH, Wang JP, Wu CQ et al (2020) Damage behaviors of unidirectional CFRP in orthogonal cutting: a comparison between single- and multiple-pass strategies. Compos Part B: Eng 185:107774. https://doi.org/10.1016/j.compositesb.2020.107774

29. Meng Q, Cai J, Cheng H, Zhang K (2020) Investigation of CFRP cutting mechanism variation and the induced effects on cutting response and damage distribution. Int J Adv Manufact Technol 106:2893–2907. https://doi.org/10.1007/s00170-019-04667-1

30. Xu J, Deng Y, Wang C, Liang G (2021) Numerical model of unidirectional CFRP in machining: development of an amended friction model. Compos Struct 256:113075. https://doi.org/10.1016/j.compstruct.2020.113075

31. Abena A, Essa K (2019) 3D micro-mechanical modelling of orthogonal cutting of UD-CFRP using smoothed particle hydrodynamics and finite element methods. Compos Struct 218:174–192. https://doi.org/10.1016/j.compstruct.2019.03.037

32. Feng Y, Jianming W, Feihong L (2012) Numerical simulation of single particle acceleration process by SPH coupled FEM for abrasive waterjet cutting. Int J Adv Manufact Technol 59:193–200. https://doi.org/10.1007/s00170-011-3495-z

33. Du M, Wang H, Dong H et al (2020) Numerical research on kerf characteristics of abrasive waterjet machining based on the SPH-DEM-FEM approach. Int J Adv Manufact Technol 111:3519–3533. https://doi.org/10.1007/s00170-020-06340-4

34. Liu X, Tang P, Geng Q, Wnag X (2019) Effect of abrasive concentration on impact performance of abrasive water jet crushing concrete. Shock Vibration 2019:1–18. https://doi.org/10.1155/2019/3285150

35. Wenjun G, Jianming W, Na G (2011) Numerical simulation for abrasive water jet machining based on ALE algorithm. Int J Adv Manufact Technol 53:247–253. https://doi.org/10.1007/s00170-010-2836-7

36. Shahverdi H, Zohoor M, Mousavi SM (2011) Numerical simulation of abrasive water jet cutting process using the SPH and ALE methods. Int J Adv Design Manufact Technol 5:43–50

37. Kaddour AS, Hinton MJ, Smith PA, Li S (2013) Mechanical properties and details of composite laminates for the test cases used in the third world-wide failure exercise. J Compos Mater 47(20-21):2427–2442. https://doi.org/10.1177/0021998313499477

38. Theory Manual LS-DYNA (2019) Livermore Software Technology Corporation. Livermore, CA

39. Chang FK, Chang KU (1987) A progressive damage model for laminated composites containing stress concentrations. J Compos Mater 21(9):834–855. https://doi.org/10.1177/002199838702100904

40. Chang FK, Chang KU (1987) Post-failure analysis of bolted composite joints in tension or shear-out mode failure. J Compos Mater 21(9):809–833. https://doi.org/10.1177/002199838702100903

41. Steinberg DJ (1987) Spherical explosions and the equation of state of water. Lawrence Livermore Natl Lab:1–8. https://doi.org/10.2172/6766676

42. Hextow AS4 carbon fiber datasheet (2014) Hexcel Corp.

43. Kawabata S (1990) Measurement of the transverse mechanical properties of high-performance fibers. J Text Inst 81(4):432–447. https://doi.org/10.1080/00405009008658721

44. Yan X, Reiner J, Bacca M, Altintas Y, Vaziri R (2019) A study of energy dissipating mechanisms in orthogonal cutting of UD-CFRP composites. Compos Struct 220:460–472. https://doi.org/10.1016/j.compstruct.2019.03.090

45. Yamamoto G, Koizumi K, Okabe T (2019) Tensile strength of unidirectional carbon fiber-reinforced plastic composites. Strength Mater. https://doi.org/10.5772/intechopen.90272

46. Minakuchi S, Niwa S, Takagaki K, Takeda N (2016) Composite cure simulation scheme fully integrating internal strain measurement. Compos Part A: Appl Sci Manufact 84:53–63. https://doi.org/10.1016/j.compositesa.2016.01.001

47. Wang DH, Ramulu M, Arola D (1995) Orthogonal cutting mechanisms of graphite/ epoxy composite. Part II: multi-directional laminate. Int J Machine Tools Manufact 35(12):1639–1648. https://doi.org/10.1016/0890-6955(95)00015-P

48. Schindelin J, Arganda-Carreras I, Frise E, Kaynig V, Longair M, Pietzsch T, Preibisch S, Rueden C, Saalfeld S, Schmid B, Tinevez JY, White DJ, Hartenstein V, Eliceiri K, Tomancak P, Cardona A (2012) Fiji: an open-source platform for biological-image analysis. Nat Methods 9(7):676–682. https://doi.org/10.1038/nmeth.2019